Development of Low-power and High-accuracy Wireless EEG Transmission System Using Compressed Sensing with an EEG Basis

Daisuke Kanemoto*, Eichi Takimoto, and Tetsuya Hirose
Graduate School of Engineering, Osaka University, Suita, Japan
*dkanemoto@eei.eng.osaka-u.ac.jp

***Abstract*—Achieving power savings while maintaining accuracy is essential for wireless electroencephalogram (EEG) measurement devices, enabling them to be lighter with smaller batteries and longer operating times. To meet this requirement, we developed a wireless EEG transmission system that utilizes compressed sensing (CS) with random undersampling to achieve high-accuracy reconstruction while reducing sensing and transmission power. As a key feature of the implemented system, we designed and employed a suitable basis from previously obtained EEG signals for the block sparse Bayesian learning algorithm. Measurements showed that our system achieved significant power savings with a compression ratio of 6, consuming only 72 μW, which is lower than that reported in the latest CS-based study. Notably, despite the reduced power consumption, we reduced the normalized mean square error to 0.116, achieving more than twice the reconstruction accuracy reported in the previous study.**

***Index Terms*—Compressed sensing, electroencephalogram (EEG), EEG basis, high reconstruction accuracy, low-power.**

I. Introduction

Healthcare technologies, including those for the early detection of Alzheimer's disease [1], [2], and brain technologies such as brain-computer interfaces that connect the brain to a computer [3], [4], are attracting increasing attention. To enable the practical use of these technologies in everyday life, it is essential to develop compact, long-lasting devices, such as wireless electroencephalogram (EEG) devices that can operate for extended periods without burdening the user (e.g., [5]). Therefore, reducing power consumption is crucial to enable a smaller battery and extend operational time to realize easy-to-use wireless EEG measurement devices. As everyone knows, power-saving technologies in integrated circuits have indeed advanced significantly. However, due to recent slowdowns in semiconductor microfabrication, achieving further power reductions using conventional signal processing methods has become challenging (e.g., [6]).

Power is consumed during each sampling, and a significant amount of power is used whenever data are sent wirelessly in EEG measurements. Therefore, compressed sensing (CS) [7], which compresses information while sensing it, is attracting increasing attention as one of the power-saving technologies. Among CS methods, those that use random undersampling achieve compression by subsampling signals with randomly selected samples [8]. This approach simplifies the compression process, providing significant benefits for circuit integration and power efficiency. Therefore, random undersampling can reduce the power consumption of many EEG measurement circuits and systems (e.g., [9]–[11]).

In general, achieving high compression can significantly reduce power consumption. However, in CS, reconstruction accuracy especially decreases for highly compressed signals if the signal sparsity is insufficient, as sparsity is utilized in the reconstruction process. Therefore, despite using CS, achieving both high accuracy and power saving remains challenging. To address this challenge, a theoretical method was proposed that achieves high-accuracy reconstruction for highly compressed signals by generating a suitable basis using previously obtained signals, with a focus on signal similarity [12]. In this study, we designed a CS-based wireless EEG transmission system utilizing EEG basis (EEGB), generated by considering similarity to the previously obtained EEG signals. Then, we implemented the CS-based system that enables high-accuracy reconstruction under high compression. By evaluating its operation on an actual device, we confirmed that it achieves both high reconstruction accuracy and reduced power consumption.

The remainder of this study is organized as follows: Section II describes the CS theory and similarity-based basis. Section III discusses the designed low-power and high-accuracy wireless EEG transmission system using CS and EEGB. Section IV presents measurement results on actual EEG signal transmission. Finally, Section V concludes the study.

II. Background of CS and Signal Similarity-based Basis Generation

A. Basics of CS

Fig. 1 illustrates the basic principle of CS. The color depth indicates the numerical size of each element. The white elements indicate zeros, and each element is normalized by the maximum value, with the highest value shown in black. The CS theory is utilized to obtain a signal vector $\mathbf{x} \in \mathbb{R}^N$, which is *k*-sparse in a basis matrix $\mathbf{\Psi} \in \mathbb{R}^{N \times P}$. Here, *k*-sparse implies that only k ($<< P$) elements of the coefficient vector $\mathbf{s} \in \mathbb{R}^P$, indicating that $\mathbf{x} = \mathbf{\Psi}\,\mathbf{s}$, are nonzero. In this example, $\mathbf{\Psi}$ is represented using a square matrix with $N = P = 12$,

This work was supported by JSPS KAKENHI Grant Number JP23K18463 and JP24K02914.

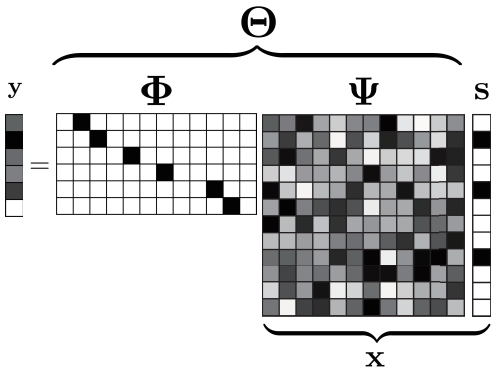

Fig. 1. Compression of the signal $\mathbf{x}$ using random undersampling for measurement matrix $\mathbf{\Phi}$ to produce a low-dimensional compressed vector $\mathbf{y}$. In CS, the reconstruction accuracy significantly depends on the basis matrix that enables the sparse representation of the vector $\mathbf{x}$ as $\mathbf{s}$.

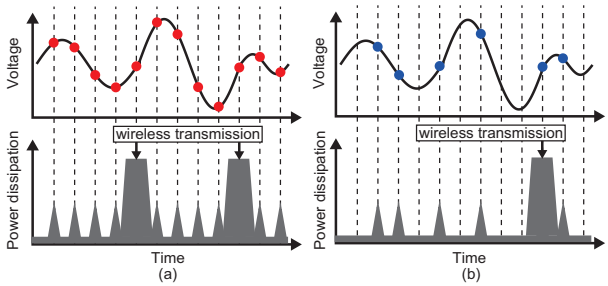

Fig. 2. Compared to equally spaced sampling, random undersampling reduces the number of sampling cycles and the number of radio transmissions.

and sparsity of $\mathbf{s}$ is $k = 3$. Various forms of $\mathbf{\Psi}$ exist, including the discrete cosine transform (DCT) [13] and the Gabor basis [14], which are classical basis matrices. Additionally, there is a method for creating a basis that uses the characteristics of the target signal (e.g., [15]). A key feature of this study is the direct use of the characteristics of previously obtained signals as a basis in the implemented system, as detailed in Sec.II-B.

The compressed signal $\mathbf{y} \in \mathbb{R}^M$ can be expressed as:

$$\mathbf{y} = \mathbf{\Phi x} = \mathbf{\Phi \Psi s} = \mathbf{\Theta s}, \tag{1}$$

where $\mathbf{\Phi}$ is an $M \times N$ measurement matrix. Various $\mathbf{\Phi}$ matrices exist (e.g., [16], [17]). This study focuses on random undersampling matrices as measurement matrices, which enable power savings (e.g., [18]–[21]). Random undersampling matrices are matrices where each row contains exactly one element with a value of 1, while all other elements are 0, where 0 represents white and 1 represents black. Additionally, they have the characteristic that if there is a 1 at row i and column j, then the 1 in row i+1 appears in a column after j+1. The matrix-vector product of a random undersampling matrix and the signal vector $\mathbf{x}$ represents acquiring the components of $\mathbf{x}$ through random and intermittent sampling. Fig. 2(a) and (b) show the circuit operations and power consumption during uniform sampling and random intermittent sampling. Random undersampling not only reduces the amount of wireless transmission but also allows for power savings by limiting the number of samples, enabling significantly greater power reduction compared to uniform sampling, while also simplifying circuit implementation. In this study, $\frac{N}{M}$ is defined as the compressed ratio (CR); thus, for example, when $M = 6$, the $CR = 2$.

Next, reconstruction is discussed. Here, $\mathbf{y}$ is a known vector, and $\mathbf{\Phi}$ and $\mathbf{\Psi}$ are known matrices. Thus, we define $\mathbf{\Theta} = \mathbf{\Phi}\ \mathbf{\Psi}$ as the sensing matrix [22]. (1) is underdetermined because the length of $\mathbf{y}$ is smaller than that of $\mathbf{s}$. Therefore, several reconstruction algorithms such as orthogonal matching pursuit (OMP) [23] and block sparse Bayesian learning (BSBL) [24] have been employed for solving the problems by utilizing $\mathbf{\Theta}$ and $\boldsymbol{y}$ to realize a sparse vector $\mathbf{s}$.

B. Signal similarity-based basis generation

The vector $\mathbf{x}$ has a block/sparse structure for signals in nature, such as biological signals [25]. Subsequently, with a suitable $\mathbf{\Psi}$, we can assume that $\mathbf{s}$ can be represented by g blocks as:

$$\mathbf{s} = [\underbrace{s_1, \cdots, s_{d_1}}_{\mathbf{s}_1^{\mathrm{T}}}, \cdots, \underbrace{s_{d_{g-1}+1}, \cdots, s_{d_g}}_{\mathbf{s}_g^{\mathrm{T}}}]^{\mathrm{T}}. \tag{2}$$

Among the g blocks, only the j ($j \ll g$) blocks are nonzero; however, their locations are unknown. Various reconstruction algorithms, such as the BSBL algorithm, benefit from the structure to achieve high accuracy [26]. In particular, due to its high reconstruction accuracy, the BSBL algorithm is widely used as a reconstruction method in many CS applications.

Generally, there is often a high degree of similarity between the target signal and previously obtained signals, and research has been conducted to leverage this property in CS (e.g., [27]). Additionally, by applying this property, it has been found that by selectively consolidating and arranging only highly correlated signals for generating signal similarity-based basis matrix to realize block/sparse structure in sparse vector $\mathbf{s}$, an optimal and compact basis for reconstruction using the BSBL algorithm can be efficiently generated [12].

III. Developed System with CS and EEGB

A. Generation of EEGB from EEG signals

We used signal similarity to create a basis matrix suitable for high-compression signal reconstruction of the BSBL algorithm. Similarity can be confirmed in various ways. In this design, the mean frequency of the histogram was calculated, and EEG signals with the most frequent values were arranged to form a basis matrix, $\mathbf{\Psi}_{\mathrm{EEG}}$, which is called EEGB. In creating the $\mathbf{\Psi}_{\mathrm{EEG}}$, we used FP1-F7 channel data from the CHB-MIT scalp EEG database [28], with each segment spanning 3 s. The data, originally sampled at 256 sample/s (SPS), were converted to 200 SPS, resulting in $N = 600$ samples per segment. Additionally, as a preprocessing step, DC offset was removed from all segment data, and segments with values exceeding 150 μV were excluded to avoid potential artifact contamination. After excluding seizure segments, we selected

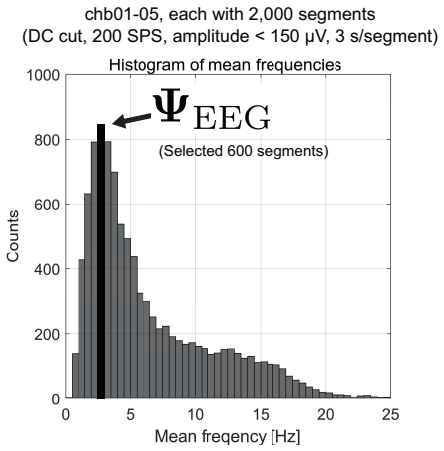

Fig. 3. Mean frequency was calculated for the EEG data from chb01 to chb05 (2,000 segments each). The basis matrix $\mathbf{\Psi}_{\mathrm{EEG}}$ was generated using the 600 segments with the highest frequencies ranging from 2.5 to 3 Hz.

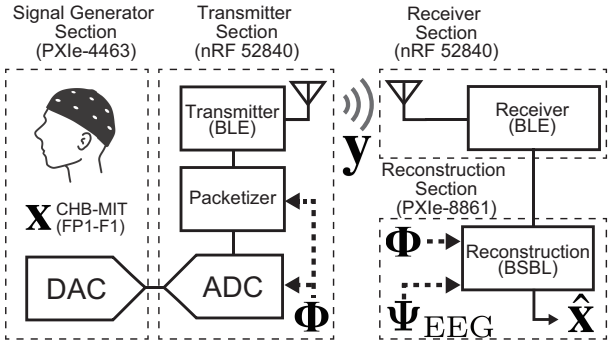

Fig. 4. An overview of our designed EEG transmission system and testbench, comprising four sections: Signal Generator, Transmitter, Receiver, and Reconstruction. Microcontroller of transmitter uses $\mathbf{\Phi}$ to realize random undersampling. The receiver uses the $\mathbf{\Phi}$ and $\mathbf{\Psi}_{\mathrm{EEG}}$ for reconstruction.

2,000 segments from each of the subjects chb01 to chb05. Here, EEG signals from subjects chb01 to chb05 are considered previously acquired data, not from the target subject to be measured. For experiments to evaluate our designed system, EEG data from a different subject were used, as explained in the next subsection. Fig. 3 shows a histogram of 10,000 segments of EEG signals arranged in order of mean frequency. A peak in the range of 2.5 Hz to 3 Hz was observable. We arranged 600 columns of EEG signals positioned at this peak and generated $\mathbf{\Psi}_{\mathrm{EEG}}$. This operation is not limited to EEG signal reconstruction in the 2.5–3 Hz range. $\mathbf{\Psi}_{\mathrm{EEG}}$, constructed by leveraging frequently occurring EEG signals with a mean frequency in this range, is expected to exhibit high similarity to the input signals.

B. Designed System

Fig. 4 shows an overview of our designed EEG measurement system and the testbench, comprising four sections: the Signal Generator, Transmitter, Receiver, and Reconstruction Sections. For the EEG signals in the Signal Generator Section, we used the FP1-F7 channel data from subject chb14 in the CHB-MIT scalp EEG database, downsampled to 200 SPS, and then divided into 3 s segments for use as test data. The DC offset and amplitude of the signal were adjusted to a suitable level, considering the input range of the analog-to-digital converter (ADC) in the Transmitter Section. The data were output from the PXIe-4463 (National Instruments), which serves as a digital-to-analog converter (DAC).

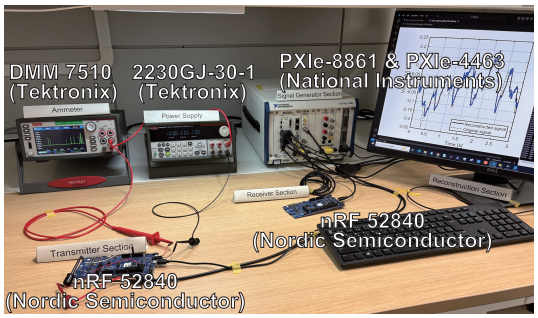

Fig. 5. Photograph of the system used for verification. The system can perform reconstruction and power measurement while operating.

The Transmitter Section uses a general-purpose microcontroller, nRF52840 (Nordic Semiconductor), which supports Bluetooth Low Energy (BLE), and integrates an ADC and a packetizer. The timing of the AD conversion was performed intermittently using a pre-created $\mathbf{\Phi}$. The packetizer and wireless module also perform operations based on the $\mathbf{\Phi}$, enabling efficient generation and wireless transmission of the compressed signal $\mathbf{y}$ while reducing the number of operations.

In this verification, nRF 52840 was also used in the Receiver Section. The received $\mathbf{y}$ is reconstructed in the Reconstruction Section consisting of PXIe-8861 (National Instruments), used as a PC with Xeon CPU and memory 16 GB RAM. All signal processing related to signal acquisition and reconstruction was performed using Python 3. The reconstruction process uses the same $\mathbf{\Phi}$ from the Transmitter Section, along with $\mathbf{\Psi}_{\mathrm{EEG}}$, to obtain the reconstructed signal $\hat{\mathbf{x}}$ using the BSBL algorithm.

IV. Evaluation our Developed System

Fig. 5 shows a photo of the experimental environment used to realize the system block in Fig. 4. This study adopted a CR of 6 to demonstrate that high-accuracy reconstruction is achievable even at high compression. We used 100 segments of the test EEG signal from subject chb14, creating five patterns of random undersampling matrices for analysis. Therefore, we experimentally verified the reconstruction accuracy through 500 iterations. In Fig. 5, the distance between the Transmitter and Receiver Sections is intentionally kept close for photographic purposes. We confirmed, however, that no issues occurred even with a separation of at least 5 m.

The power supply for the nRF 52840 in the Transmitter Section was set to 3.3V and provided by the 2230J-30-1 (Tektronix). An ammeter (DMM7510 (Tektronix)) capable of displaying 7.5 digits was placed between the power supply and the nRF 52840. In this measurement, it was crucial to accurately measure the steady current, the single-shot current

TABLE I
PERFORMANCE OF WIRELESS EEG TRANSMISSION SYSTEMS.

	This work	T. Miyata et al. [11]	C. Chen et al. [29]	X. Liu et al. [30]
CS-based Acquisition	**Yes ($CR = 6$)**	Yes ($CR = 4$)	No	Yes ($CR = 8^{(1)}$)
Power Consumption [μW]	**72**$^{(2)}$	97$^{(2)}$	90$^{(3)}$	230$^{(4)}$
Sampling Rate [SPS], Resolution [bit]	**200, 12**	256, 12	300, 12	500, 10
Measured Average NMSE (Iterations)	**0.116 (500)**	0.24 (100)	N/A	N/A
Reconstruction Algorithm, Basis	**BSBL, EEGB**	OMP, DCT	N/A	ℓ_1-norm base, Not reported

$^{(1)}$ At 500 SPS, $^{(2)}$ General-purpose Microcontroller (nRF 52840), $^{(3)}$ ASIC (2 ADCs + TX + XO + PMU), $^{(4)}$ ASIC (PGA + ADC + CS Core + TX)

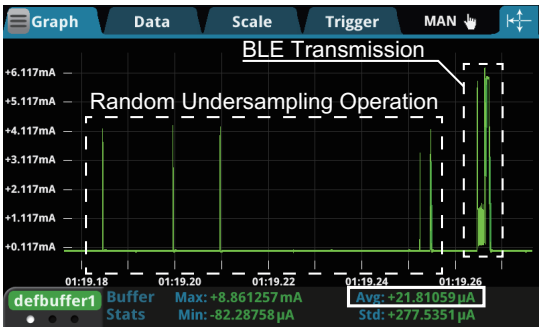

Fig. 6. Results of measuring current during operation. The power consumption for BLE communication can be confirmed after intermittent sampling by random undersampling. The average current consumption was 21.8μA.

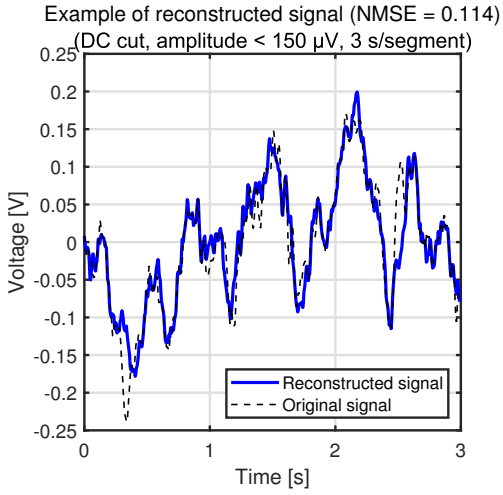

Fig. 7. This is one of the reconstructed waveforms using the BSBL algorithm and $\mathbf{\Psi}_{\mathrm{EEG}}$, with the NMSE of 0.114 for this segment, close to the average NMSE obtained from the measurement results of 500 iterations. The reconstructed waveform closely matches the original signal.

during AD conversion, and the current during BLE transmission. The ammeter was chosen for its ability to measure currents ranging from tens of mA to several μA. Fig. 6 shows the measured current waveform, in which the current consumption occurs at the timing of AD conversion and BLE transmission. A significant amount of current consumption occurs when the data are transmitted wirelessly. The average current over 120 s was 21.8 μA. Therefore, the measured power consumption was 72μW.

In this study, we used the normalized mean square error (NMSE) index, as shown in the following formula, to evaluate the accuracy of the reconstruction:

$$\mathrm{NMSE} = \frac{\|\mathbf{x} - \hat{\mathbf{x}}\|_2^2}{\|\mathbf{x}\|_2^2}. \tag{3}$$

In this study, we cut the DC component to suppress its influence and calculated the NMSE. A lower NMSE indicates a smaller difference between the original signal $\mathbf{x}$ and the reconstructed signal $\hat{\mathbf{x}}$, suggesting higher reconstruction accuracy. At a CR of 6, the average NMSE across 500 reconstruction iterations was 0.116. This result indicates that the difference between the original and reconstructed signals was minimal, demonstrating high reconstruction accuracy even with repeated iterations around 500. Fig. 7 illustrates an example of reconstruction, in which NMSE is 0.114, and the reconstructed signal waveform utilizing signal similarity at CR = 6 is close to the original signal.

Table I compares the power consumption and other system characteristics of our designed system with those of recently proposed systems. [11] is an example of a system that has adopted random undersampling and implemented a transmission system, which reduced power consumption to 97μW. However, our developed system achieved a $CR = 6$, reducing power consumption to 72μW. Despite this power reduction, the NMSE was kept at 0.116, which is less than half of the NMSE in [11], indicating a reconstruction accuracy more than twice as high. Unlike ASIC-based studies [29], [30], the proposed system with a general-purpose microcontroller achieves superior power efficiency, which is also significant.

V. CONCLUSION

In this study, we designed a wireless EEG transmission system using the EEG signal similarity basis $\mathbf{\Psi}_{\mathrm{EEG}}$, achieving high-accuracy reconstruction, high compression, and power saving. We developed the system using the general-purpose microcontroller nRF52840, applying random undersampling. The study results yielded a significant reduction in power consumption by setting CR = 6, achieving 72μW in actual measurements. Despite this power reduction, the NMSE was maintained at 0.116, achieving significantly higher accuracy in reconstruction than previous CS study. These results address the challenge of achieving both high compression and high-accuracy reconstruction in CS, demonstrating the potential for further advancements in sensor accuracy and power efficiency.

REFERENCES

[1] T. Musha, H. Matsuzaki, Y. Kobayashi, Y. Okamoto, M. Tanaka, and T. Asada, "EEG markers for characterizing anomalous activities of cerebral neurons in NAT (neuronal activity topography) method," *IEEE Trans. Biomed. Eng.*, vol. 52, no. 8, pp. 2332–2338, Aug. 2013.

[2] K. AlSharabi, Y. B. Salamah, A. M. Abdurraqeeb, M. Aljalal, and F. A. Alturki, "EEG signal processing for Alzheimer's disorders using discrete wavelet transform and machine learning approaches," *IEEE Access*, vol. 10, pp. 89 781–89 797, Jan. 2022.

[3] X. Gu, Z. Cao, A. Jolfaeim, P. Xu, D. Wu, T. P. Jung, and C. T. Lin, "EEG-based brain-computer interfaces (BCIs): A survey of recent studies on signal sensing technologies and computational intelligence approaches and their applications," *IEEE/ACM Trans. Comput. Biol. Bioinf.,*, vol. 18, no. 5, pp. 1645–1666, Sep. 2021.

[4] D. Wu, Y. Xu, and B. L. Lu, "Transfer learning for EEG-based brain-computer interfaces: A review of progress made since 2016," *IEEE Trans. Cogn. Dev. Syst.*, vol. 14, no. 1, pp. 4–19, Mar. 2022.

[5] J. Sabio, N. S. Williams, G. M. McArthur, and N. A. Badcock, "A scoping review on the use of consumer-grade EEG devices for research," *PLoS One*, vol. 19, no. 3, p. Art. no. e0291186, 2024.

[6] M. T. Bohr and I. A. Young, "CMOS scaling trends and beyond," *IEEE Micro*, vol. 37, no. 6, pp. 20–29, Nov. 2017.

[7] D. L. Donoho, "Compressed sensing," *IEEE Trans. Inf. Theory*, vol. 52, no. 4, pp. 1289–1306, Apr. 2006.

[8] Y. Okabe, D. Kanemoto, O. Maida, and T. Hirose, "Compressed sensing EEG measurement technique with normally distributed sampling series," *IEICE Trans. Fundamentals*, vol. E105-A, no. 10, pp. 1429–1433, Oct. 2022.

[9] K. Mii, D. Kanemoto, and T. Hirose, "0.36μw/channel capacitively-coupled chopper instrumentation amplifier in EEG recording wearable devices for compressed sensing framework," *Jpn. J. Appl. Phys.*, vol. 63, 03SP54, 2024.

[10] R. Matsubara, D. Kanemoto, and T. Hirose, "Reducing power consumption in LNA by utilizing EEG signals as basis matrix in compressed sensing," in *Proc. IEEE Int. Symp. Circuits Syst. (ISCAS)*, May 2024, pp. 1–5.

[11] T. Miyata, D. Kanemoto, and T. Hirose, "Random undersampling wireless EEG measurement device using a small TEG," in *Proc. IEEE Int. Symp. Circuits Syst. (ISCAS)*, May 2023, pp. 1–5.

[12] D. Kanemoto and T. Hirose, "EEG measurements with compressed sensing utilizing EEG signals as the basis matrix," in *Proc. IEEE Int. Symp. Circuits Syst. (ISCAS)*, May 2023, pp. 1–5.

[13] Z. Zhang, T.-P. Jung, S. Makeig, and B. D. Rao, "Compressed sensing of EEG for wireless telemonitoring with low energy consumption and inexpensive hardware," *IEEE Trans. Biomed. Eng.*, vol. 60, no. 1, pp. 221–224, Jan. 2013.

[14] M. Mohsina and A. Majumdar, "Gabor based analysis prior formulation for EEG signal reconstruction," *Biomed. Signal Process. Control*, vol. 8, no. 6, pp. 951–955, Nov. 2013.

[15] K. Nagai, D. Kanemoto, and M. Ohki, "Applying K-SVD dictionary learning for EEG compressed sensing framework with outlier detection and independent component analysis," *IEICE Trans. Fundamentals*, vol. E104-A, no. 9, pp. 1375–1378, Sep. 2021.

[16] X. Chen, Z. Yu, S. Hoyos, B. M. Sadler, and J. Silva-Martinez, "A sub-nyquist rate sampling receiver exploiting compressive sensing," *IEEE Trans. Circuits Syst. I, Reg. Papers*, vol. 58, no. 3, pp. 507–520, Mar. 2011.

[17] F. Chen, A. P. Chandrakasan, and V. M. Stojanovic, "Design and analysis of a hardware-efficient compressed sensing architecture for data compression in wireless sensors," *IEEE J. Solid-State Circuits*, vol. 47, no. 3, pp. 744–756, Mar. 2012.

[18] D. Kanemoto, S. Katsumata, M. Aihara, and M. Ohki, "Compressed sensing framework applying independent component analysis after undersampling for reconstructing electroencephalogram signals," *IEICE Trans. Fundamentals*, vol. E103-A, no. 12, pp. 1647–1654, Dec. 2020.

[19] S. Katsumata, D. Kanemoto, and M. Ohki, "Applying outlier detection and independent component analysis for compressed sensing EEG measurement framework," in *Proc. IEEE Biomed. Circuits Syst. Conf. (BioCAS)*, Oct. 2019, pp. 1–4.

[20] T. Miyata, D. Kanemoto, and T. Hirose, "Utilizing previously acquired BSBL algorithm parameters in the compressed sensing framework for EEG measurements," in *Proc. IEEE Int. Conf. Consum. Electron. (ICCE)*, Jan. 2024, pp. 1–5.

[21] R. Tsunaga, D. Kanemoto, and T. Hirose, "Noise-masking cryptosystem using watermark and chain generation for EEG measurement with compressed sensing," in *Proc. IEEE Int. Conf. Consum. Electron. (ICCE)*, jan. 2024, pp. 1–6.

[22] M. Mangia, F. Pareschi, V. Cambareri, R. Rovatti, and G. Setti, *Adapted Compressed Sensing for Effective Hardware Implementations*, 2018.

[23] J. A. Tropp and A. C. Gilbert, "Signal recovery from random measurements via orthogonal matching pursuit," *IEEE Trans. Inf. Theory*, vol. 53, no. 12, pp. 4655–4666, Dec. 2007.

[24] Z. Zhang and B. D. Rao, "Extension of SBL algorithms for the recovery of block sparse signals with intra-block correlation," *IEEE Trans. Signal Process.*, vol. 61, no. 8, pp. 2009–2015, Apr. 2013.

[25] Y. C. Eldar, P. Kuppinger, and H. Bölcskei, "Block-sparse signals : uncertainty relations and efficient recovery," *IEEE Trans. Signal Process*, vol. 58, no. 6, pp. 3042–3054, Jun 2010.

[26] R. G. Baraniuk, V. Cevher, M. F. Duarte, and C. Hegde, "Model-based compressive sensing," *IEEE Trans. Inf. Theory*, vol. 56, no. 4, pp. 1982–2001, Apr. 2010.

[27] M. Fira and L. Goras, "Comparison of inter-and intra-subject variability of P300 spelling dictionary in EEG compressed sensing," *Int. J. Adv. Comput. Sci. Appl.*, vol. 7, no. 10, pp. 366–371, Oct. 2016.

[28] A. Shoeb, *Application of Machine Learning to Epileptic Seizure Onset Detection and Treatment*, Sep. 2009.

[29] C. Chen, J. Yang, H. Wang, Z. Cao, S. Kananian, K. Chen, and A. S. Y. Poon, "A 90-μw penny-sized 1.2-gram wireless EEG recorder with 12-channel FDMA transmitter for month-long continuous mental health monitoring," in *Proc. IEEE Symp. VLSI Technol. Circuits*, Jun. 2022, pp. 248–249.

[30] X. Liu, A. G. Richardson, and J. V. der Spiegel, "An energy-efficient compressed sensing-based encryption scheme for wireless neural recording," *IEEE J. Emerg. Sel. Topics Circuits Syst.*, vol. 11, no. 2, pp. 405–414, Jun. 2021.